Crossover from localized to diffusive water dynamics in carbon nanohorns: a comprehensive quasielastic neutron scattering analysis

Marie-Claire Bellissent-Funel
LLB, CEA, CNRS, Université Paris-Saclay, CEA Saclay, 91191 Gif-sur-Yvette, France

Katsumi Kaneko
Center for Energy and Environmental Science, Shinshu University, 1-17-1 Wakasato, Nagano, Japan

Tomonori Ohba
Graduate School of Science, Chiba University, 1-33 Yayoi, Inage, Chiba 263-8522, Japan

Marie-Sousai Appavou, Antti J. Soininen, and Joachim Wuttke*
Forschungszentrum Jülich GmbH, JCNS at MLZ, Lichtenbergstraße 1, 85747 Garching, Germany
(Dated: February 20, 2016)

Incoherent neutron scattering by water confined in carbon nanohorns was measured with the backscattering spectrometer SPHERES, and analyzed in exemplary breadth and depth. Quasielastic spectra admit delta-plus-Kohlrausch fits over a wide q and T range. From the q and T dependence of fitted amplitudes and relaxation times, however, it becomes clear that the fits do not represent a uniform physical process, but that there is a crossover from localized motion at low T to diffusive α relaxation above about 210–230 K. The crossover temperature increases with decreasing wavenumber, which is incompatible with a thermodynamic strong-fragile transition. Extrapolated diffusion coefficients $D(T)$ indicate that water motion is at room temperature about 2.5 times slower than in the bulk; in the supercooled state this factor becomes smaller. At even higher temperatures, where the α spectrum is essentially flat, a few percent of the total scattering goes into a Lorentzian with a width of about 1.6 μeV, probably due to functional groups on the surface of the nanohorns.

I. INTRODUCTION

Confinement to narrow pores can alter material properties substantially and in sometimes surprising ways. Recent discoveries include the formation of a high-pressure phase at ambient pressure,[1] and the synthesis of metallic sulphur chains in carbon nanotubes.[2] Capillary thermodynamics results in depressed or increased freezing points.[3] Freezing and melting are often accompanied by a considerable hysteresis. Furthermore, below the freezing point there remain typically a few liquid-like monolayers between a frozen core and the pore wall. This division in surface and bulk, however, fails for the smallest pores, with diameters below 3–4 nm. In such confinement, material structures are qualitatively different from the bulk, and phase transitions are smeared or vanish altogether.[4]

Confined *water* is of particular interest because of numerous applications from biology to geology but also because of theoretical speculations that see confined water as a proxy for the inaccessible deeply supercooled state of bulk water. Confined water forms defective cubic ice instead of the hexagonal bulk phase, or can be supercooled into an amorphous state. In either case, hydrogen bonding is enhanced with respect to the bulk.[5]

The molecular *dynamics* of confined water has been studied principally by quasielastic neutron scattering (QENS),[6–10] dielectric relaxation,[11,12] and nuclear magnetic resonance.[13–15] Translational motion in narrow pores is found to be slower than in the bulk. Upon supercooling the molecular dynamics slows down more and more, in ways similar to bulk glass formation.

Confinement acts through surface interactions, reduced dimensionality, finite-size effects, and other geometrical constraints. To disentangle these influences, it is necessary to systematically study different systems. Initial research had concentrated on nanopores with hydrophilic surfaces. More recently, emphasis has been put on comparison with hydrophobic systems like silica with functionalized surfaces[16,17] or carbon nanotubes.[18–23] Differences between water properties at hydrophobic and hydrophilic interfaces have important implications in applications such as microfluidics or the development of biomaterials. Translational motion in narrow pores with hydrophilic surface is found to be slower than in the bulk. Upon supercooling the molecular dynamics slows down more and more, in ways similar to bulk glass formation. However, in carbon nanotubes with hydrophobic surface, where interaction is not possible, water is found to flow up to five orders of magnitude faster than predicted by the Hagen-Poiseuille equation.[24] A drastic change in hydrogen-bond connectivity results in fluid-like mobility of nanotube water at temperatures far below the nominal freezing point.[25]

In this work, we use QENS to investigate the molecular dynamics of water in single-walled carbon nano*horns*. Their main difference from open-ended nano*tubes* is the different topology. Besides, they provide more heterogeneous environments for the water, which can form a smaller cluster (trimer or tetramer) at the inner tip site, and larger clusters (pentamers to ocotamers) in the tubular regions.

Our original intention was to compare the dynamics of water in carbon nanohorns with related systems; principally, of course, with carbon nanotubes. However, closer scrutiny showed that results in this field depend so strongly on data analysis procedures that a comparison across research groups is currently not feasible. Therefore, we focus on methodological questions, and report in unusual detail on the data analysis.

Our experiments were carried out in April 2010. Since then, data analysis was interrupted and resumed several times, taking altogether more than 5 years. In the following we do our best to present our analysis as a rational narrative. This shall however not hide the fact that the logic of our work, as of any similar study, is not deductive, but heuristic. Any data analysis, as straightforward as it might appear in the final write-up, depends on a considerable number of technical choices and physical assumptions. Many other choices and assumptions had to be tried out until we slowly converged towards the analysis presented here, which we consider to be about as simple it can possibly be made, but no simpler than the complexity of the experimental method and the rich information content of the data set require.

II. METHODS

A. Experiment

Carbon nanohorn powder (type *ox-NH* of Ref. 26) was produced by laser ablation of pure graphite, followed by 1 h exposition to O_2 at 673 K for opening the horns. After 0.5 h the O/C ratio, assessed by XPS, was 0.05. An individual nanohorn consists of a graphene sheet shaped into a single-walled tube with a conical cap. The average tubular diameter, which depends slightly on preparation details, is about 2.8 nm. The nanohorns aggregate in *dahlia*-shaped particles.

The nanohorn powder was exposed to water vapor until a water load of 0.51 g/g was reached. This level is in good agreement with the specific volume of the intra-tube space (0.36 $\mathrm{cm^3 g^{-1}}$) plus the interstitial pore volume (0.11 $\mathrm{cm^3 g^{-1}}$),[27] and with reported water isotherms.[26] The sample material was transferred into an Al container of top-sealed hollow-cylinder type.[28] The external diameter was 25 mm, and the sample volume between the concentric Al tubes had a thickness of 1.25 mm, resulting in a transmission of about 0.9.

Unfortunately, there was no way to measure reference spectra of dry nanohorns: we had not enough material to prepare two samples, and within a few days of beam time it was not possible to load or unload the water from the sample. This compels us to estimate the scattering contribution from the nanohorn matrix by an extrapolation procedure, explained below in Sect. III A.

Experiments were carried out at the high-resolution neutron backscattering spectrometer SPHERES.[29] Thirteen detectors cover the wavenumber range $q = 0.22 \ldots 1.8$ Å^{-1}. The first four detectors (up to $q = 0.45$ Å^{-1}, conventionally designated as "small-angle detectors") are not exactly in backscattering geometry, which results in a shifted, broadened, and asymmetric resolution function.[30] To favor statistics, especially at low temperatures where quasielastic scattering is weak and appears only in a small energy window around the elastic line, we did not use the full dynamic range of SPHERES of ± 31 μeV, but set the Doppler velocity amplitude to 2.9 m/s to cover a dynamic range of -19.1...+19.0 μeV. This implies that relaxation times must not be much shorter than $\hbar/19$ μeV $\simeq 35$ ps for quasielastic spectra not to appear mostly flat in our experiment.

The sample was cooled in 10 steps from 277 to 4 K in a cryofurnace. Measurements at 175, 200, 225, and 277 K were replicated upon heating, then two more measurements were undertaken at 292 and 312 K. All replicated spectra coincide within statistical accuracy with the original ones. We conclude that there is no dependency on thermal history, in contrast to what might have been expected from a recent study of carbon nanotubes.[23] In the following, replicated data are merged with the original ones, and the thermal history is not considered further.

From our 4 K measurements, we find a signal-to-noise ratio between 465:1 and 1343:1 in the large-angle detectors, and between 354:1 and 567:1 in the small-angle detectors. The resolution full-width at half maximum is between 0.663 and 0.695 μeV in the large-angle detectors, and between 0.85 and 1.26 μeV in the small-angle detectors.

B. Data reduction

Using the standard SPHERES data reduction program `SLAW`,[31] raw neutron counts are binned into histogram channels with a width of 0.24 μeV and normalized to the accumulation time per channel, yielding raw spectra $S_{\mathrm{raw}}(q,\omega,T)$ in arbitrary units. Further data treatment, visualization and fitting is done with `Frida2`.[32]

Inevitably, S_{raw} comprises a background $B(q,\omega,T)$. We determine an affine-linear $B(q,\omega) = b_q + c_q\omega$ by fitting the extreme tails ($|\omega| > 16$ μeV) of the spectra $S(q,\omega,T_0)$ at $T_0 \coloneqq 4$ K. We keep $B(q,\omega)$ fixed for all T and ω, thereby neglecting the T dependence of background channels that involve scattering by the sample. This is far better than freely fitting $B(q,\omega,T)$, which would cause an unmanageable parameter degeneracy in the case of very broad quasielastic spectra. Our further analysis will be based on normalized spectra

$$S_{\mathrm{nor}}(q,\omega,T) \coloneqq \frac{S_{\mathrm{raw}}(q,\omega,T)}{\int \mathrm{d}\omega \left[S_{\mathrm{raw}}(q,\omega,T_0) - B(q,\omega)\right]}. \quad (1)$$

C. Fitting

When directly analyzing scattered intensities, we use the background-corrected variant

$$S_{\mathrm{corr}}(q,\omega,T) \coloneqq S_{\mathrm{nor}}(q,\omega,T) - B(q,\omega). \tag{2}$$

When fitting, however, we do *not* remove $B(q,\omega)$ from the experimental data (which would impair visual inspection on a logarithmic intensity scale), but include it in the fit function

$$S_{\mathrm{fit}}(q,\omega,T) = S(q,\omega,T) \otimes R(q,\omega) + B(q,\omega). \tag{3}$$

Furthermore the fit involves a convolution with the instrumental resolution $R(q,\omega) \coloneqq S_{\mathrm{corr}}(q,\omega,T_0)$. The theoretical scattering law $S(q,\omega,T)$ shall be called the *fit kernel*.

To fit the spectra S_{nor} with a fit function S_{fit} as introduced in (3), we minimize

$$\chi^2 = \sum_i^n \frac{1}{n-n_{\mathrm{par}}-1} \cdot \frac{[S_{\mathrm{nor}}(\omega_i) - S_{\mathrm{fit}}(\omega_i)]^2}{\sigma^2_{\mathrm{nor}}(\omega_i) + \sigma^2_{\mathrm{fit}}(\omega_i)}, \tag{4}$$

where n is the number of energy bins ω_i, and n_{par} is the number of fit parameters. Weighing χ^2 with the inverse of the variance σ^2_{nor} is the standard way to account for the statistical uncertainty of the empirical data S_{nor}. Besides σ^2_{nor} there is another term σ^2_{fit}, which rarely, if ever, is mentioned in the description of scattering data analyses. It accounts for the uncertainty of S_{fit} due to its dependence on the measured resolution function, and is computed by straightforward error propagation from the Poissonian error estimate for $R(q,\omega)$.

Fits that look satisfactory in a plot of $\log S_{\mathrm{nor}}$ vs ω all have $\chi^2 \lesssim 3$. Most good fits have $1 < \chi^2 < 1.5$. If $1.5 < \chi^2 < 3$, we would normally depend on visual inspection to assess whether the shortcomings of the fit are due to instrumental imperfections or to systematic deviations from the assumed model. However, in a field where results seem to depend on analysis procedures, the first concern ought to be reproducibility. To use an objective, albeit arbitrary, criterion we reject fits when $\chi^2 > 2$.

The convolution integral in (3)

$$S(\omega) \otimes R(\omega) \coloneqq \int_{-\infty}^{+\infty} \mathrm{d}\omega'\, S(\omega-\omega')R(\omega') \tag{5}$$

is usually computed as a Riemann sum

$$S(\omega) \otimes R(\omega) \simeq \Delta\omega \sum_j S(\omega-\omega_j)R(\omega_j). \tag{6}$$

However, this is bound to result in unacceptable discretization errors if S has a sharp peak so that it varies strongly within one spectral bin $\Delta\omega$.[33] To avoid such errors, we proceed as proposed in App. B of Ref. 34, computing

$$\begin{aligned} &S(\omega) \otimes R(\omega) \\ &= \sum_j \int_{\omega_j-\Delta\omega/2}^{\omega_j+\Delta\omega/2} \mathrm{d}\omega'\, S(\omega-\omega')R(\omega') \\ &\simeq \sum_j R(\omega_j) \int_{\omega_j-\Delta\omega/2}^{\omega_j+\Delta\omega/2} \mathrm{d}\omega'\, S(\omega-\omega') \\ &= \sum_j R(\omega_j) \left[P\left(\omega-\omega_j+\frac{\Delta\omega}{2}\right) - P\left(\omega-\omega_j-\frac{\Delta\omega}{2}\right)\right], \end{aligned} \tag{7}$$

where

$$P(\omega) \coloneqq \int_0^{\omega} \mathrm{d}\omega' S(\omega') \tag{8}$$

is the primitive of the fit kernel S.

D. Spectral model

The measured spectra contain an elastic contribution from the nanohorns matrix. Following the generic rule that differences of noisy data are to be avoided we make no attempt to subtract an elastic line from the observed spectra, but rather include it in our fit model,

$$S(q,\omega,T) = F_{\mathrm{horns}}(q,T)\delta(\omega) + F_{\mathrm{water}}(q,T)S_{\mathrm{water}}(q,\omega,T). \tag{9}$$

Amplitudes F may be fixed at values that will be determined in Sect. III A from elastic or total scattering intensities. The water spectrum may also include a delta line, and therefore has the generic form

$$S_{\mathrm{water}}(q,\omega,T) = (1-c)\delta(\omega) + cQ(\omega,q,T) \tag{10}$$

with a quasielastic amplitude $c(q,T)$. The quasielastic spectrum has the standard normalization $\int \mathrm{d}\omega\, Q = 1$.

In QENS studies of confined water,[7,8,21] it has become well established that the simplest adequate model for $Q(\omega)$ is the Kohlrausch spectrum

$$K(\omega,\tau,\beta) = \frac{1}{\pi}\int_0^{\infty} \mathrm{d}t\, \cos(\omega t) \exp\left(-(t/\tau)^{\beta}\right). \tag{11}$$

This is consistent with the longstanding practice of fitting α relaxation in viscous liquids by stretched exponential time-correlation functions,[35] and also with a time-dependent study of water dynamics.[36]

Compared to a Gaussian ($\beta = 2$), or even to a Lorentzian ($\beta = 1$), the Kohlrausch spectrum with typical stretching exponents $\beta \ll 1$ is noticeable for combining broad wings with a sharp central peak. In consequence, the discretization problem described above in connection with Eq. (6) is particularly acute for Kohlrausch fits. We therefore compute the resolution with the experimental resolution following Eq. (7). The

required primitive (8) of K is provided with high accuracy by the numeric library `libkww`.[34]

It is common practice to report numeric values of τ in form of the mean relaxation time

$$\langle\tau\rangle = \int \mathrm{d}t\, K(\omega,\tau,\beta) = \frac{\tau}{\beta}\Gamma(1/\beta). \tag{12}$$

We go one step further and use $c, \langle\tau\rangle, \beta$ instead of c, τ, β as independent parameters in our spectral fits. This will enable us in Sect. III C to perform fits with a q-independent mean relaxation time, while the line shape, expressed by β, is allowed to depend on q.

E. Degenerate parameters

For any given q and T, the delta-plus-Kohlrausch model (9–11) has three free parameters, c, τ, and β. For a free fit to yield reliable estimates of all these three parameters it is necessary that the nontrivial curvature of the quasielastic line falls well into the experimental frequency window. Otherwise degeneracies will impair the accuracy of parameters:[33]

In the case of very slow relaxation, τ is large compared to the inverse of the spectrometer resolution $\delta\omega$. Therefore $\tau\omega \gg 1$ for all $\omega \gtrsim \delta\omega$. The Kohlrausch spectrum (11) has the large-ω expansion[37]

$$K(\omega,\tau,\beta) = \frac{\tau}{\pi}\sum_{k=1}^{\infty}(-1)^{k-1}\frac{\Gamma(k\beta+1)}{\Gamma(k+1)}\sin\frac{k\beta\pi}{2}(\omega\tau)^{-k\beta-1}. \tag{13}$$

The singularity at $|\omega| \to 0$ results in a sharp, resolution-limited peak that is indistinguishable from elastic scattering. This prevents an independent determination of the quasielastic amplitude c. If quasielastic intensity appears in the wings of the resolution function, then it is dominated by the $k = 1$ term. This power-law approximation

$$K(\omega,\tau,\beta) \simeq \tau^{-\beta}\frac{\Gamma(\beta+1)}{\pi}\sin\frac{\beta\pi}{2}\omega^{-\beta-1} \tag{14}$$

makes the amplitude c degenerate with the parameter τ that only appears in the linear factor $\tau^{-\beta}$. Furthermore, due to the steep decrease $\omega^{-\beta-1}$ there will only be a small frequency range where the quasielastic intensity outshines the instrumental background. Such a restricted frequency range will not allow a reliable determination of the power-law exponent, hence of the stretching parameter β.

In the opposite case of very fast relaxation, τ is large compared to the inverse of the maximum frequency covered by the spectrometer. Therefore $\tau\omega \ll 1$ for all experimental ω. The Kohlrausch spectrum has the small-ω Taylor expansion

$$K(\omega,\tau,\beta) = \frac{\tau}{\pi\beta}\sum_{k=0}^{\infty}(-1)^{k}\frac{\Gamma\left((2k+1)/\beta\right)}{\Gamma(2k+1)}(\omega\tau)^{2k}. \tag{15}$$

The leading order is a constant,

$$K(\omega,\tau,\beta) \simeq \frac{\tau}{\pi\beta}\Gamma\left(1/\beta\right), \tag{16}$$

which makes the parameters τ and β degenerate. Their specific combination happens to coincide with the expression (12) for the mean Kohlrausch relaxation time, so that the flat quasielastic intensity

$$K(\omega,\tau,\beta) \simeq \frac{\langle\tau\rangle}{\pi} \tag{17}$$

could in principle be used to determine $\langle\tau\rangle$, regardless of the stretching exponent. However, the smaller $\langle\tau\rangle$, the more critically such data analysis would depend on two assumptions: First, on the temperature independence of the background signal, assumed in (3), and second, on extrapolated amplitudes $F_{\mathrm{horns}}(q,T)$ and $F_{\mathrm{water}}(q,T)$ in (9), needed for determining the quasielastic amplitude c from the elastic amplitude $1-c$ in (10). Therefore, one should not rely on spectral determinations of $\langle\tau\rangle$ unless the spectrum shows at least *some* curvature from the second-order term in (15).

III. RESULTS

A. Elastic and total intensities

To start the quantitative data analysis, let us consider the elastic and total scattering intensities as function of T and q. Later on, this analysis will prove helpful in that it allows to constrain amplitude parameters in spectral fits. Fig. 1 shows the elastic component of the background-corrected scattering (2),

$$I(q,T) \coloneqq S_{\mathrm{corr}}(q,0,T)/S_{\mathrm{corr}}(q,0,T_0), \tag{18}$$

and the total scattering

$$J(q,T) \coloneqq \int \mathrm{d}\omega\, S_{\mathrm{corr}}(q,\omega,T) \tag{19}$$

as function of T for representative values of q. The integration limits in (19) are given by the experimental ω range of ± 19 μeV. By construction both functions have a zero-temperature limit of $I(q,0) = J(q,0) = 1$.

The main feature of the figure is a crossover of I and J between two limiting cases, indicated by solid lines. These lines show elastic scattering as expected for a harmonic solid,

$$F(q,T) = f(q)\exp[-2(W(q,T) - W(q,0))], \tag{20}$$

where

$$2W(q,T) = w(q)\left[\frac{2T}{\Theta}D_1\left(\frac{\Theta}{T}\right) + \frac{1}{2}\right] \tag{21}$$

involves the Debye temperature Θ, and the Debye function D_1.[38] In each of the three panels of Fig. 1, the lower

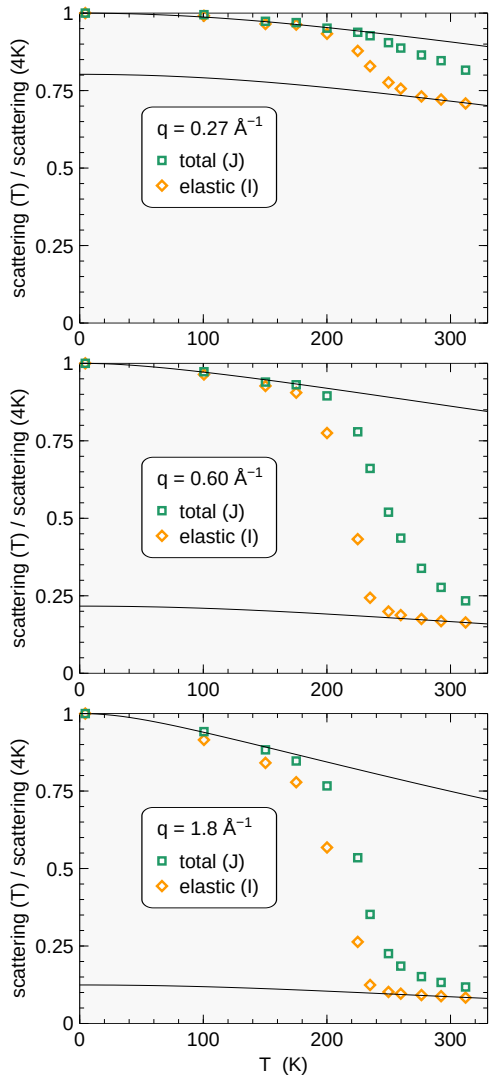

FIG. 1. Scattering intensity versus T for three representative values of q. Diamonds: elastic intensity $I(q,T)$. Squares: total intensity $J(q,T)$ within the experimental window of ± 19 μeV. Lower line: Debye-Waller factor of the matrix, assuming $\Theta = 1000$ K. Upper line: lower line plus Debye-Waller factor of ice, with $\Theta = 220$ K.

line represents the elastic scattering $F_{\mathrm{horns}}(q,T)$ by the nanohorn matrix alone whereas the upper line shows the combined elastic scattering $F_{\mathrm{tot}}(q,T) = F_{\mathrm{horns}}(q,T) + F_{\mathrm{water}}(q,T)$ by the nanohorns and the confined water in the solid-like low-T limit. Appendix A describes how these lines were fitted.

The relative scattering contribution $f_{\mathrm{horns}}(q) := F_{\mathrm{horns}}(q,0)$ of the nanohorns amounts to between 0.12 and 0.22 of the total scattering, except at the four lowest q where it rises to values between 0.46 and 0.85. These large values are primarily due to coherent small-angle scattering by the nanohorns but there may also be a contribution from unresolved quasielastic water scattering.[39]

The crossover of I and J from the low-T limit F_{tot} to the high-T limit F_{horns} is of course due to the onset of quasielastic scattering by the water: When the water spectrum broadens with increasing T, the elastic intensity $I_{\mathrm{water}}(q,T) := I(q,T) - F_{\mathrm{horns}}(q,T)$ decreases towards zero. And when the line becomes so broad that most of the scattering involves energy transfers that exceed our experimental window, the total intensity $J_{\mathrm{water}}(q,T)$ also decreases towards zero. In other words, Fig. 1 shows onset of structural α relaxation at two different time scales, the one given by the instrumental resolution of 0.66...0.69 μeV (for the nine large-angle detectors, otherwise 0.85...1.26 μeV), the other given by the chosen scan limit of 19 μeV. This time-dependent onset of α relaxation is also known as the dynamic glass transition.

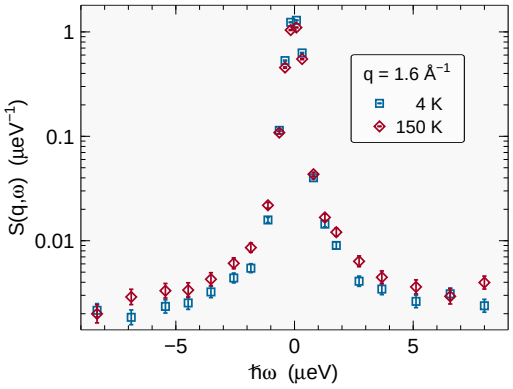

FIG. 2. Spectra at $q = 1.6$ Å^{-1}, $T = 4$, 150 K. Plotted in a reduced spectral range of ± 9 μeV and with a non-equidistant binning in order to highlight the statistical significance of the quasielastic scattering at 150 K.

According to Fig. 1, quasielastic scattering starts at exceptionally low temperatures: At 100 K and 1.8 Å^{-1}, the elastic scattering $I(q,T)$ is significantly lower than the total scattering $J(q,T)$, which implies that some scattering goes into inelastic channels. We considered the possibility that this were an experimental artifact but could not come up with any plausible mechanism. It rather seems that there is indeed quasielastic broadening at temperatures as low as 100 K. This is fully confirmed by direct inspection of quasielastic spectra. For visual clarity, Fig. 2 shows a spectrum at 150 K, but even at 100 K there is some quasielastic scattering that cannot be explained by statistical fluctuations.

B. Dynamic regimes

Fig. 3 shows the scattering intensity $S(q,\omega;T)$, integrated over a certain inelastic $|\omega|$ interval, as function of temperature. On heating from 4 to 175 K, weak quasielastic scattering appears at large q. On further heating, the scattering intensity increases strongly, due to quasielastic broadening of the central peak. A maximum is reached at about 220 to 260 K, depending on q. At

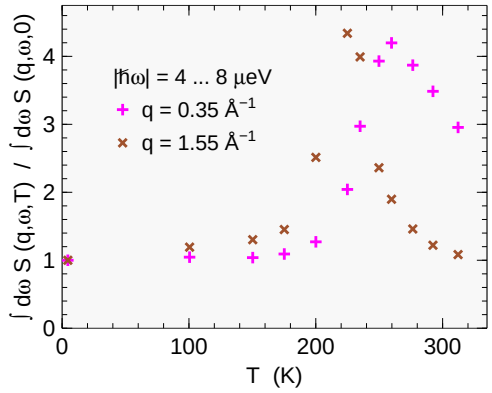

FIG. 3. Scattering intensity for $|\omega|$ between 4 and 8 μeV for two representative detectors. Data are normalized to the background measured at 4 K.

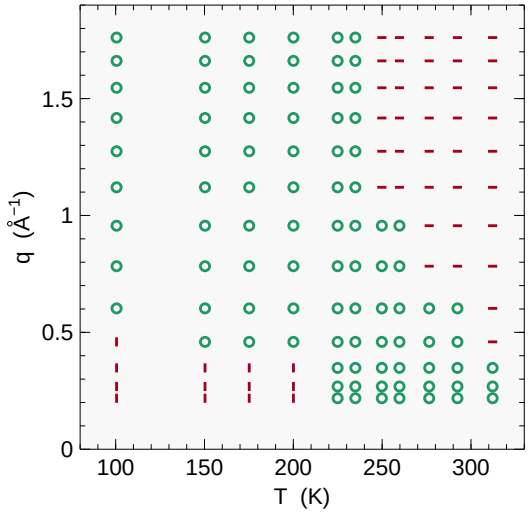

FIG. 4. Location of measured spectra in the q, T plane. In the low-T, small-q region (|), relaxational dynamics is too slow or/and too weak to be resolved by SPHERES. In the intermediate region (○), quasielastic scattering from α relaxation is well resolved; these spectra will be used in the analysis of Sect. III C and III D. In the high-T, large-q region (−), relaxation dynamics is so fast that the α-relaxation spectrum is almost flat within the frequency range of SPHERES; however, there appears some additional quasielastic scattering from slow relaxation that will be analyzed in Sect. III E.

higher temperatures, the registered intensity decreases because the relaxational spectrum becomes *so* broad that only a small part of it falls into the considered frequency window.

This strong dependence of the quasielastic width on q and T has for consequence that by far not all the measured 156 spectra (12 temperatures [besides the resolution scan at 4 K] times 13 detectors) admit reliable fits of spectral line shapes. In the course of our data analysis, we heuristically developed two criteria which spectra to exclude from quasielastic fits:

First, to identify cases where relaxational dynamics is too slow or/and too weak to be reasonably resolved by SPHERES, we fitted experimental spectra at given q, T with the minimal one-parameter model

$$S(q, \omega; T) = a(q, T)\delta(\omega), \tag{22}$$

inserted in (3) just as any other fit model. If the resulting χ^2, obtained according to (4), are no larger than 1.1 times the χ^2 of the standard delta-plus-Kohlrausch fit (9–11), then the spectrum is excluded from further quasielastic fits. This concerns 13 spectra at low T and small q.

Second, to delimit the opposite extreme where α relaxation is so fast that the quasielastic spectrum is almost flat within the frequency range of SPHERES, we impose an arbitrary 15% limit for the variation of the average intensity in two $|\omega|$ intervals: If

$$\frac{\langle S(q, \omega; T)\rangle_{|\omega| \text{ in } (16\pm2)\ \mu\text{eV}}}{\langle S(q, \omega; T)\rangle_{|\omega| \text{ in } (8\pm2)\ \mu\text{eV}}} < 0.85, \tag{23}$$

then the spectrum is excluded from further quasielastic fits. This concerns 38 spectra at high T and large q. However, we will come back to these spectra in Sect. III E, where we discover a fast relaxational component at $\omega \ll 6$ μeV on top of the otherwise almost flat α-relaxation spectrum.

The resulting map of excluded and retained spectra as function of q and T is shown in Fig. 4.

C. Spectral fits

The delta-plus-Kohlrausch model (9–11) has three parameters, c, $\langle\tau\rangle$, and β, which may all depend on q and T. If the quasielastic spectrum is well resolved within the experimental frequency window, it is possible to obtain all three parameters from a least-squares fit. If on the other hand a spectrum is too narrow or too broad to be well resolved, then free fits suffer from parameter degeneracies, as described in Sect. II E. Meaningful conclusions can only be derived conditional on physical assumptions in form of parameter constraints. Such constraints must be constructed heuristically: perform free fits, spot trends, formulate a trend as a constraint, and tentatively impose it to a new round of fits.

Fig. 5 shows exemplary spectra at three intermediate temperatures and at two wavenumbers, corresponding to the smallest and the largest scattering angle covered by regular backscattering detectors. One sees clearly, especially at 235 K, that there is a distinct elastic line on top of the quasielastic spectrum. All spectra are perfectly represented by unconstrained three-parameter fits with the delta-plus-Kohlrausch model (9–11). For most q, T these fits are almost indistinguishable from the constrained fits we shall motivate in the following.

Fig. 6 reports the quasielastic amplitude $c(q, T)$ obtained from unconstrained spectral fits with the delta-plus-Kohlrausch model. Up to 225 K, $c(q, T)$ increases systematically with q and with T. At 235 K a plateau

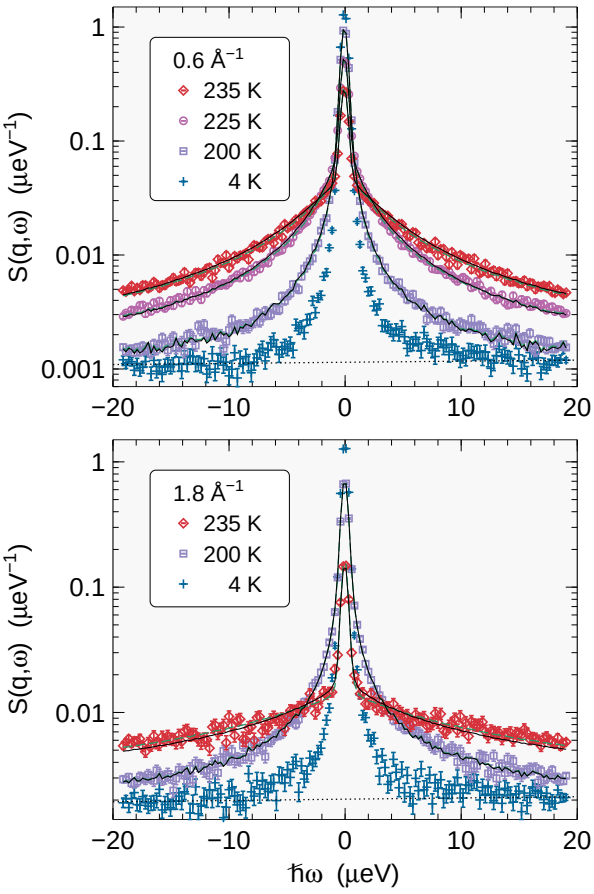

FIG. 5. Spectra at three intermediate temperatures and for two different wavenumbers. Also shown is the instrumental resolution measured at 4 K. Dotted lines represent the affine-linear background $B(q,\omega)$. Green dashed lines are unconstrained three-parameter fits with the delta-plus-Kohlrausch model; they are largely covered by black solid lines that represent our final fits obtained under stringent constraints [fixed $\beta(q)$; fixed $c = 1$ for $T \geq 235$ K; q-independent $\tau(T)$ for $T \leq 200$ K].

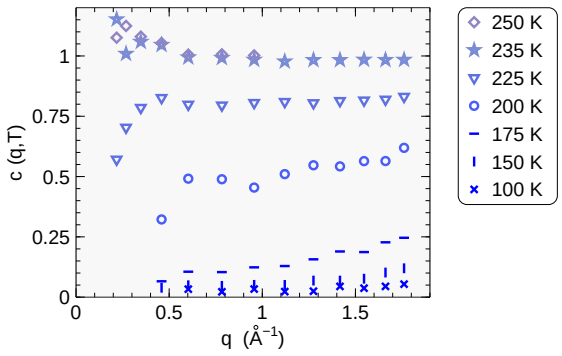

FIG. 6. Quasielastic amplitude $c(q,T)$ obtained from unconstrained spectral fits with the delta-plus-Kohlrausch model, shown as function of q for different T between 100 and 250 K. These data suggest the constrained $c = 1$ for $T \geq 235$ K. For $T \leq 225$ K, compare the improved $c(q,T)$ in Fig. 9.

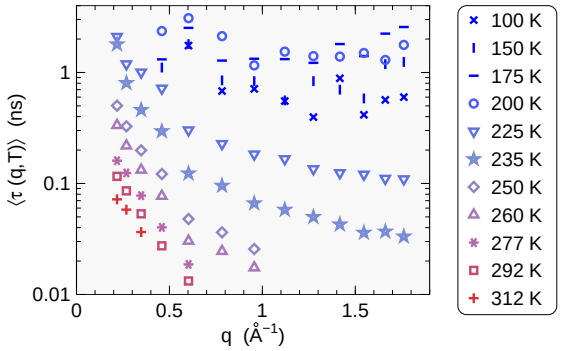

FIG. 7. Mean relaxation time $\langle\tau(q,T)\rangle$ from spectral fits with the delta-plus-Kohlrausch model, with c constrained as per Fig. 6. These data suggest to constrain τ as T independent for $T \lesssim 200$ K. For $T \geq 225$ K, compare the improved $\langle\tau(q,T)\rangle$ in Fig. 10.

value close to 1 is reached. In the small-angle detectors, nonphysical values above 1 are observed. Let us remind that the determination of $c(q,T)$ from the water spectra (10) depends on the extrapolated numeric values $F_{\text{horns}}(q,T)$ and $F_{\text{water}}(q,T)$ in (9). An inaccuracy at small q, where there scattering is dominated by elastic scattering from the nanohorns, is not surprising. Conversely, we take the fit result $c \to 1$ for large q and $T \gtrsim 235$ K as a confirmation that our fit model (9,10) is adequate and that our determination of $F_{\text{horns}}(q,T)$ and $F_{\text{water}}(q,T)$ in Sect. III A is overall very reliable. We feel therefore entitled to impose the constrained $c(q,t) = 1$ for $T \geq 235$ K to the next round of spectral fits.

Fig. 7 reports the mean relaxation times $\langle\tau(q,T)\rangle$ obtained from these fits. For temperatures of 225 K and above, and for all q except in the first detector at 0.21 Å^{-1}, there is a perfectly systematic dependence of $\langle\tau\rangle$ on q and T. On the other hand, fit outcomes up to 200 K seem to fluctuate at random; in particular, there is no systematic q dependence. This motivates us to treat $\langle\tau(T)\rangle$ as a q-independent fit parameter in the next round of spectral fits for $T \leq 200$ K, which means we must simultaneously fit all spectra obtained at one temperature.

Fig. 8 reports the Kohlrausch stretching exponent $\beta(q,T)$ obtained from fits with constrained c or $\langle\tau\rangle$, dependent on temperature. Not shown are fit results for very low or very high temperatures, which exhibit only random fluctuations. There is a clear overall trend that β decreases with increasing q, except at $q = 0.22$ Å^{-1} where β has anomalously low values. In Appendix B we will argue that this is an instrumental artifact. Accordingly, we will exclude this detector at the smallest scattering angle from further analysis. In a decent approximation, the q dependence of β can be represented by a straight line. The $\beta(q)$ defined by this line will be imposed in our last round of spectral fits, in addition to the above derived constraints of c and $\langle\tau\rangle$. As shown above in Fig. 5, all these constraints have little to no influence upon fitted

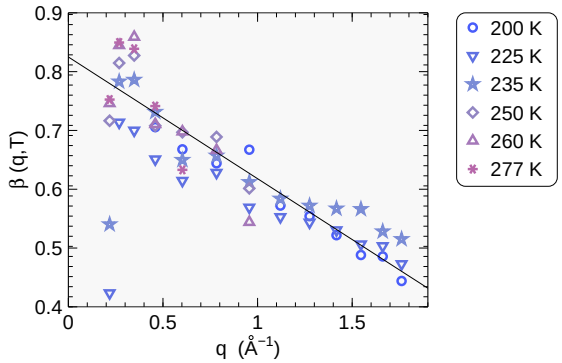

FIG. 8. Kohlrausch stretching exponent $\beta(q,T)$ from spectral fits with the delta-plus-Kohlrausch model, with c and $\langle\tau\rangle$ constrained as per Figs. 6 and 7. For temperatures not shown, fitted $\beta(q,T)$ exhibit only random fluctuations. The straight line is a global fit to all shown data points, except at 0.21 Å^{-1}, which are considered outliers (see App. B).

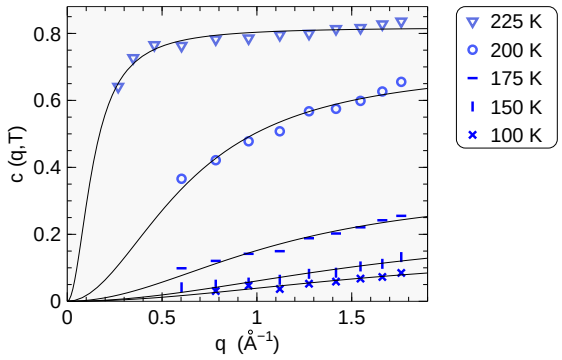

FIG. 9. Quasielastic amplitude $c(q,T)$ obtained from spectral fits with the delta-plus-Kohlrausch model with q-independent $\langle\tau(T)\rangle$ and T-independent, fixed $\beta(q)$. Solid lines are fits with (24).

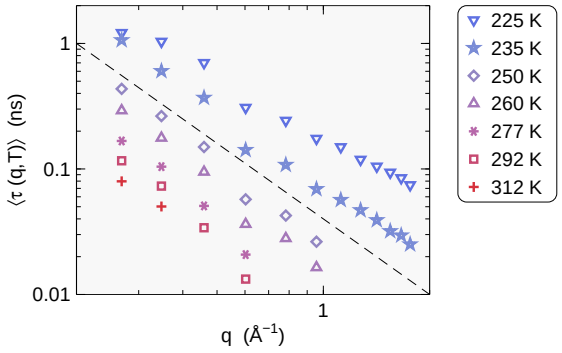

FIG. 10. Mean relaxation time $\langle\tau(q,T)\rangle$ from spectral fits with the delta-plus-Kohlrausch model, with $c = 1$ for $T \geq 235$ K, and fixed $\beta(q)$ given by the straight-line fit of Fig. 8. In contrast to the preceding figures, this one has a logarithmic q axis. The dashed line indicates a power law q^{-2}.

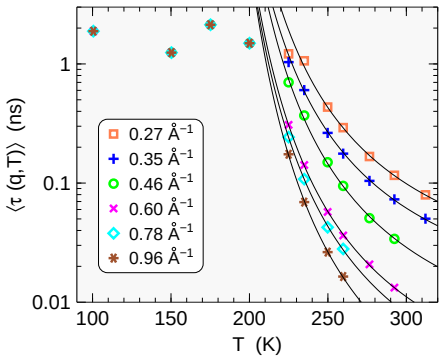

FIG. 11. Mean relaxation time $\langle\tau(q,T)\rangle$ as in Fig. 10, plotted as function of temperature. Solid lines are Vogel-Fulcher fits [restricted to relaxation times $\langle\tau(q,T)\rangle < 0.8$ ns; data points logarithmically weighted], resulting in a global parameter $T_\infty = 152$ K.

line shapes.

D. Fitted parameters

Fig. 9 improves upon Fig. 6 by reporting quasielastic amplitudes $c(q,T)$ that have been determined under the above derived stringent constraints for $\langle\tau(T)\rangle$ and $\beta(q)$. As expected, the fit constraints have greatly reduced the random fluctuations of the unconstrained parameter c. The solid lines in Fig. 9 are fits with

$$c = c_\infty q^2/(\kappa^2 + q^2), \tag{24}$$

which is about the simplest way to interpolate between diffusion-like $c \propto q^2$ at low q and a constant c_∞ at high q.

Similarly, Fig. 10 is an improved version of Fig. 7, with mean relaxation times $\langle\tau(q,T)\rangle$ determined not only under the constrained $c = 1$ for $T \geq 235$ K, but also with fixed $\beta(q)$. The resulting q and T dependence of the fitted $\langle\tau\rangle$ is slightly more systematic. For $q \lesssim 1$ Å^{-1}, it is compatible with the power-law $\langle\tau\rangle \propto q^{-2}$ expected for diffusive motion. The weaker q dependence at larger q is probably due to some contribution from localized motion.

Finally, Fig. 11 shows the mean relaxation times $\langle\tau(q,T)\rangle$ as function of temperature T for those wavevectors q for which the analyzable temperature range according to Fig. 4 extends at least up to 277 K. At 200 K and below, the $\langle\tau(q,T)\rangle$ are q independent as imposed above, and exhibit only a weak random dependence on T. At 225 K and above, on the other hand, the $\langle\tau(q,T)\rangle$ depend strongly on both q and T. The T dependence cannot be accounted for by an Arrhenius law, but it is well fitted by a Vogel-Fulcher law

$$\langle\tau(q,T)\rangle \propto \exp\left(\frac{A(q)}{T - T_\infty}\right). \tag{25}$$

The global parameter T_∞ is extremely sensitive to which data points are included in the fit. To allow for some crossover to the low-T regime, we exclude relaxation times above 0.8 ns, and obtain $T_\infty \simeq 150$ K.

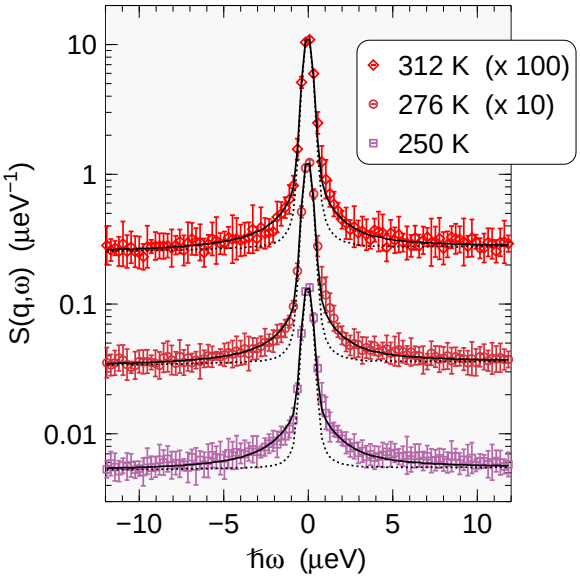

FIG. 12. Spectra at high T, averaged over the six detectors at the largest scattering angles with $q = 1.1 \ldots 1.8$ Å^{-1}, vertically shifted for clarity. Solid lines: fits with three-component kernel (27), comprising a flat relaxational contribution, an elastic contribution from the nanohorn matrix, and a Lorentzian. Dotted lines: as before, with Lorentzian amplitude set to zero.

The shortest relaxation time reported in Fig. 11 is 13 ps. This is fully consistent with our estimate in Sect. II A that spectra are *mostly flat* if relaxation times are *much shorter* than the inverse of the maximum energy shift, $\hbar/19$ μeV$\simeq$ 35 ps. Mostly flat spectra had been excluded from the above analysis per criterion (23).

E. Slow relaxation at high temperature

At high T and large q, α relaxation is so fast that spectra are mostly flat within our dynamic window of ± 19 μeV. However, this is not the full story. Besides the mostly flat α relaxation spectrum and the elastic line, there is a third contribution to $S(q,\omega)$. This contribution is not accounted for by the delta-plus-Kohlrausch model (9–11) considered so far.

The novel spectral component shows no stretching; it is well fitted by a Cauchy-Lorentz line shape

$$L(\omega,\Gamma) = \frac{\Gamma}{\pi}\frac{1}{\omega^2+\Gamma^2}. \qquad (26)$$

A minimal kernel for fitting entire spectra in the high-T regime therefore comprises three terms:

$$S(q,\omega,T) = a_0\delta(\omega) + a_1\frac{\langle\tau\rangle}{\pi} + a_2 L(\omega,\Gamma). \qquad (27)$$

The delta function represents elastic scattering by the nanohorn matrix. The constant term represents α relaxation with constant spectral intensity (17). To keep things simple, we treat $a_0(q,T)$ and $a_1(q,T)$ as free parameters, in contrast to our above analysis of α relaxation where we kept them fixed at predetermined values $F_{\mathrm{horns}}(q,T)$ and $F_{\mathrm{water}}(q,T)$.

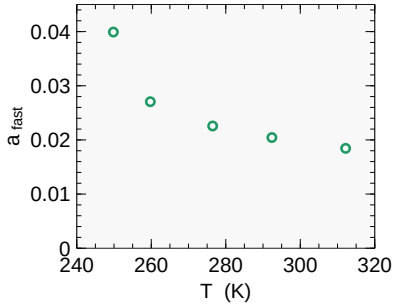

FIG. 13. Temperature dependence of the amplitude a_2 of the slow spectral component, as fitted in Fig. 12.

We could not discern any systematic q or T dependence of the line width $\Gamma(q,T)$, nor any systematic q dependence of the amplitude $a_2(q,T)$. We therefore averaged $S(q,\omega)$ over the seven largest scattering angles, and performed fits with a global parameter Γ, for which a value of 1.6 μeV is found, corresponding to a relaxation time of $\hbar/\Gamma = 0.4$ ns. Fig. 12 demonstrates the excellent quality of these fits. Fig. 13 shows that the amplitude $a_2(T)$ decreases systematically with increasing temperature.

IV. DISCUSSION

A. α relaxation and diffusion

For $T \gtrsim 235$ K, spectral fits with the delta-plus-Kohlrausch model (9–11) gave quasielastic amplitudes close to 1, which means that the observed elastic scattering can be fully attributed to the nanohorn matrix (plus a little contribution from the sample container). Since there is no elastic scattering from water, the intermediate incoherent scattering function $I(q,t)$ has a long-time limit of zero. From this we can conclude that the observed quasielastic scattering, fitted by a Kohlrausch spectrum (11), is indeed due to structural α relaxation.

In Fig. 8 we have seen that the stretching exponent β decreases from 0.77 to 0.49 with q increasing from 0.27 to 1.8 Å^{-1}. Such q dependence is well known from incoherent neutron scattering in glass-forming liquids; it is to be expected because in the limit $q \to 0$ the relaxational scattering law $S(q,\omega)$ must cross over to ordinary, memory-less diffusion with $\beta \to 1$.[40] In App. B we argue that experimental artifacts may somewhat reduce the measured β, especially at low q, which would mean that the dependence of the true, physical β on q is even more pronounced. Any such dependence is of course in conflict with ideas that there be a universal stretching exponent, let alone with a "magic" value of 3/5.[41,42]

The mean relaxation times $\langle\tau(q,T)\rangle$ shown in Figs.

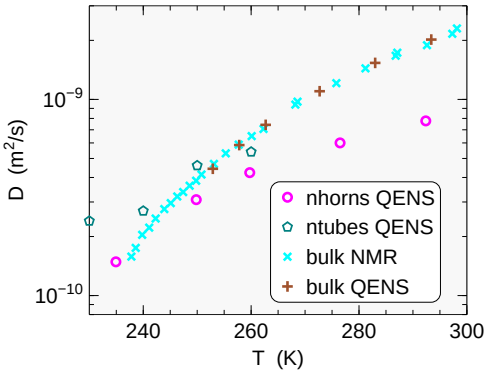

FIG. 14. Diffusion coefficient $D(T)$ of water in carbon nanohorns, from a $q \to 0$ extrapolation of our $1/(q^2\langle\tau\rangle)$. Also shown are values for single-walled carbon nanotubes[18] although we do not subscribe to the data analysis in that work, and accurate data for bulk water from NMR[43] that have recently been confirmed by QENS.[44]

10 and 11 do not factorize into functions of q and T. *A fortiori*, they are not compatible with a diffusion law

$$\langle\tau(q,T)\rangle = \frac{1}{D(T)q^2}. \tag{28}$$

However, the figures suggest that such a law holds asymptotically for $q \to 0$. This allows us the tentative determination of diffusion coefficients by extrapolating $1/(q^2\langle\tau(q,T)\rangle)$ from $q = 0.46$ and 0.35 Å^{-1} to $q^2 \to 0$. We estimate that the resulting $D(T)$ have an uncertainty of the order of 10 %. In Fig. 14 they are compared with literature data for water in other or no confinement.

Water dynamics in carbon nanotubes has been measured using the neutron spectrometer HFBS that is very similar to SPHERES.[18] Spectra were analyzed on linear intensity scales only, and fitted with a delta-plus-Lorentzian kernel. Line widths were allowed to vary with q, and amplitudes were allowed to vary as well, but were neither discussed nor documented. Given these profound differences in data analyses, it is remarkable that obtained diffusion coefficients differ by less than a factor of 2, and follow the same temperature dependence, except at $T \leq 230$ K where a data interpretation in terms of α relaxation is highly questionable, as we will argue below.

Furthermore, Fig. 14 shows the accurately known diffusion coefficient of bulk water.[43,44] In comparison, at 292 K the motion of water confined in nanohorns is about 2.4 times slower. This difference diminishes on cooling: the diffusion coefficient of bulk water decreases more rapidly so that the difference between bulk and confined water approximately vanishes around 240 K. However, we warn against taking this result too literally. Around 240 K, our D may contain a substantial admixture from the localized motion to be discussed in the next section.

B. Crossover to localized relaxation

At $T \leq 225$ K, the quasielastic amplitude $c(q,T)$, shown in Figs. 6 and 9, is definitively smaller than 1. Following the logic of the first paragraph of the preceding Sect. IV A, the intermediate scattering function has a finite long-term limit $I(q, t \to \infty) > 0$. This means that molecules remain confined to a finite environment of their initial location; their relaxational dynamics, seen through quasielastic scattering, is *localized*. In ordered systems, incoherent scattering from rotations or other localized modes is described by one or a few Lorentzians, and oscillations of the amplitude as function of q provide insight into the modes' geometry.[45] In our disordered system, the quasielastic spectra are substantially stretched, in accord with recently reported cage correlations,[42] and oscillations of the amplitude $c(q,T)$ as function of q are averaged out.

Accordingly, the dramatic qualitative change in the temperature dependence of the mean relaxation time $\langle\tau(q,T)\rangle$ that appears in Fig. 11 at about 210–240 K is due to a crossover in the dominant quasielastic scattering mechanism from diffusive to localized relaxation. This conclusion is perfectly consistent with other neutron scattering results, like an analysis of integrated intensities from a medium-resolution spectrometer, neutron scattering intensities,[20] or QENS analyzed at fixed T,[8] which show crossover from mainly translational at low wavenumbers q to mainly rotational at high q. All this is also consistent with NMR observations of rotational motion in amorphous 'plastic ice' near interfaces.[15] How our rotation-translation crossover relates to the dielectric α-β merger[46] is less clear: It occurs at about the same temperature as the kink in the neutron scattering relaxation times,[47] but dielectric β relaxation does not normally show up in neutron spectra, except possibly[48] some fast secondary process on a $1 \ldots 10$ ns scale.

C. No fragile-strong transition

In Ref. 49 and in many later papers, some of them reporting on water in carbon nanotubes,[18,21,22] a kink in the neutron scattering relaxation time as function of temperature has been interpreted as manifestation of an otherwise unobservable *fragile-to-strong transition*. While the possible connection[50,51] of this transition with a Widom line that emanates from the phase boundary[52] between low- and high-density amorphous ice belongs to the realm of speculation, its supposed connection with relaxational dynamics implies testable predictions: The relaxation times determined on either side of the supposed transition temperature must stem from one and the same relaxation process (which furthermore must be unaffected by finite-size effects[53]), and relaxation times determined at different q must be consistent with a q-independent transition temperature.

Both tests are covered by our above data analysis.

Near the supposed transition temperature, there is a qualitatively change in the q and T dependence of fitted amplitudes c and time constants $\langle\tau\rangle$. This strongly suggests a fundamental change in the observed relaxation process. In the previous Sect. IV B we have explained this change as a crossover in the dominant scattering contribution from localized to diffusive. Independently of that interpretation we can state that there exists no fit model that works in the same way below and above a transition that manifests itself only in the temperature dependence of $\langle\tau(T)\rangle$. This alone is enough to rule out the fragile-to-strong hypothesis.

Secondly, our data analysis has shown that the transition temperature depends on q and is spread over an interval of at least 20 K, as shown in Fig. 11, which is of course incompatible with a thermodynamic phase transition. Note that most QENS reports in favor of a fragile-strong transition were based on data analyses either at just *one* arbitrarily chosen q, or on an average over detectors at widely different angles.

Similar and related arguments have been voiced since long against the fragile-strong hypothesis. The low-T branch of $\langle\tau(T)\rangle$ extrapolates to an unrealistic glass transition temperature.[47] Dielectric spectroscopy, NMR, and other methods do not yield any pronounced crossover in the α relaxation times of confined water, hydration water, or water mixtures near the supposed T_{L}.[12,54,55] provided α and β relaxation are properly distinguished.[47,56,57] A QENS analysis suggested that the appearance of a pronounced kink in $\langle\tau(T)\rangle$ may be connected with fit parameter degeneracies.[33]

D. Slow relaxation at high temperatures

In Sect. III E we reported on an unexpected, weak, but pronounced quasielastic scattering component at high temperatures, due to some process that is much slower than α relaxation. Fig. 13 shows that the amplitude $a_2(T)$ of this process decreases with increasing temperature. Slightly less convincing fits are obtained if a_2 is kept fixed and the line width $\Gamma(T)$ allowed to vary with T; in this case, $\Gamma(T)$ decreases with increasing T. We have no explanation for either temperature dependence.

Anyway, this slow process contributes only a few percent to the total scattering. Therefore it is not necessarily due to the confined water, but could also stem from a minority species. From X-ray photoelectron spectroscopy we know that the O/C ratio of our oxidized nanohorns was between 0.05 and 0.07. All oxygen is thought to be part of surface functional groups like COOH, -OH, =CO, -C-O-C-. Therefore it is not implausible that our high-T, small-ω scattering component is due to internal motion of such groups. These groups are mostly located near the nanohorn caps (where there are many pentagons, which are more unstable for oxidation, so that there are more nanoscale windows on the caps). Therefore, motion of surface functional groups and of water molecules adsorbed to them should be highly restricted.

APPENDICES

Appendix A: Fitting the harmonic limiting cases

The harmonic scattering intensities, shown as solid lines in Fig. 1, are all based on *one* global fit

$$\begin{aligned} &F_{\mathrm{horns}}(q,T)+F_{\mathrm{water}}(q,T) \to J(q,T) \text{ at 100, 150 K,} \\ &F_{\mathrm{horns}}(q,T) \qquad\qquad\qquad\quad \to I(q,T) \text{ at 292, 312 K,} \end{aligned} \tag{A1}$$

performed simultaneously for the four listed values of T and for all thirteen values of q. It is based on two assumptions: At low temperatures, there is no quasielastic scattering outside our experimental window. At high temperatures, quasielastic scattering by water is so broad that its contribution to the elastic scattering is negligible. The first assumption is unproblematic. The second one is an excellent approximations except for the lowest q.[39]

To reduce the arbitrariness of the fit, parameters were constrained as much as possible. The Debye temperatures were fixed at literature values: $\Theta_{\mathrm{horns}} = 1000$ K, as approximately known for carbon nanotubes,[58] and $\Theta_{\mathrm{water}} = 220$ K.[59] The amplitudes are constrained as $f_{\mathrm{horns}} + f_{\mathrm{water}} = 1$. As often in amorphous systems, the prefactor $w(q)$ in (21) is not simply $\propto q^2$. It rather goes into saturation, heuristically described by $w(q) = u^2q^2/(1+v^2q^2)$. We obtained the parameters $u_{\mathrm{horns}} = 2.90$ Å, $v_{\mathrm{horns}} = 2.42$ Å, $u_{\mathrm{water}} = 0.474$ Å, $v_{\mathrm{water}} = 1.23$ Å.

Appendix B: Stretching through angular averaging

In a backscattering spectrometer like SPHERES, each detector collects neutrons back-reflected from a certain analyzer area. Detectors of one type, at different scattering angles ϑ, typically see analyzer segments of different angular width $\Delta\vartheta$. For small ϑ, $q \propto \vartheta$. For diffusion, and more generally for diffusive relaxation in the limit $q \to 0$, the spectral line width goes with $\Gamma \propto \tau^{-1} \propto q^2 \propto \vartheta^2$. Since a detector covers a finite angular range, it collects a mixture of spectra with different widths. The relative width of the width distribution is $\Delta\Gamma/\Gamma = 2\Delta\vartheta/\vartheta$, which diverges for $\vartheta \to 0$.

The mixture of spectra with different Γ results in an apparent *stretching* of the observed spectrum.[30] This has nothing to do with the intrinsic, physical stretching of a scattering law $S(q,\omega)$, but may look very similar, and equally admit a Kohlrausch fit. If the scattering law is intrinsically Kohlrausch, then the mixture of different τ will result in a reduction of β.

We think that this is what happened in the detector at the smallest scattering angle, with a nominal q of 0.21 Å^{-1}. We therefore consider the unsystematically

low β at this q, shown in Fig. 8, as an instrumental artifact, and exclude this detector from the final analysis. It is also quite possible that the physical $\beta(q)$ are systematically higher than the observed ones, the more so the lower q, which would mean that the physical decrease of β with increasing q is even stronger than observed in our experiment.

ACKNOWLEDGMENT

This project has received funding from the European Union's Seventh Framework Programme for research, technological development and demonstration under the NMI3 Grant number 226507.

* To whom correspondence should be addressed, j.wuttke@fz-juelich.de

[1] K. Urita, Y. Shiga, T. Fujimori, T. Iiyama, Y. Hattori, H. Kanoh, T. Ohba, H. Tanaka, M. Yudasaka, S. Iijima, I. Moriguchi, F. Okino, M. Endo and K. Kaneko, J. Am. Chem. Soc. **133**, 10344 (2011).

[2] T. Fujimori, A. Morelos-Gómez, Z. Zhu, H. Muramatsu, R. Futamura, K. Urita, M. Terrones, T. Hayashi, M. Endo, S. Y. Hong, Y. C. Choi and D. Tománek, Nature Commun. **4**, 2162 (2013).

[3] C. Alba-Simionesco, B. Coasne, G. Dosseh, G. Dudziak, K. E. Gubbins, R. Radhakrishnan and M. Sliwinska-Bartkowiak, J. Phys. Condens. Matter **18**, R15 (2006).

[4] H. K. Christenson, J. Phys. Condens. Matter **13**, R95 (2001).

[5] J. Dore, Chem. Phys. **258**, 327 (2000).

[6] M.-C. Bellissent-Funel, S. H. Chen and J.-M. Zanotti, Phys. Rev. E **51**, 4558 (1995).

[7] J.-M. Zanotti, M.-C. Bellissent-Funel and S.-H. Chen, Phys. Rev. E **59**, 3084 (1999).

[8] M.-C. Bellissent-Funel, Eur. Phys. J. E **12**, 83 (2003).

[9] J.-M. Zanotti, M.-C. Bellissent-Funel and S.-H. Chen, Europhys. Lett. **71**, 91 (2005).

[10] S. Takahara, N. Sumiyama, S. Kittaka, T. Yamaguchi and M.-C. Bellissent-Funel, J. Phys. Chem. B **109**, 11231 (2005).

[11] R. Bergman and J. Swenson, Nature **403**, 283 (2000).

[12] J. Swenson and S. Cerveny, J. Phys. Condens. Matter **27**, 033102 (2015).

[13] S. Stapf, R. Kimmich and R.-O. Seitter, Phys. Rev. Lett. **75**, 2855 (1995).

[14] Y. Hirama, T. Takahashi, M. Hino and T. Sato, J. Coll. Interf. Sci. **184** (1996).

[15] J. B. W. Webber, Progr. Nucl. Mag. Res. Sp. **56**, 78 (2010).

[16] A. Faraone, K.-H. Liu, C.-Y. Mou, Y. Zhang and S.-H. Chen, J. Chem. Phys. **130**, 134512 (2009).

[17] J. Jelassi, T. Grosz, I. Bako, M.-C. Bellissent-Funel, J. C. Dore, H. L. Castricum and R. Sridi-Dorbez, J. Chem. Phys. **134**, 064509 (2011).

[18] E. Mamontov, C. J. Burnham, S.-H. Chen, A. P. Moravsky, C.-K. Loong, N. R. de Souza and A. I. Kolesnikov, J. Chem. Phys. **124**, 194703 (2006).

[19] K. Matsuda, T. Hibi, H. Kadowaki, H. Kataura and Y. Maniwa, Phys. Rev. B **74**, 073415 (2006).

[20] N. R. de Souza, A. I. Kolesnikov, C. J. Burnham and C.-K. Loong, J. Phys. Condens. Matter **18**, S2321 (2006).

[21] X.-Q. Chu, A. I. Kolesnikov, A. P. Moravsky, V. Garcia-Sakai and S.-H. Chen, Phys. Rev. E **76**, 021505 (2007).

[22] S. M. Chathoth, E. Mamontov, A. I. Kolesnikov, Y. Gogotsi and D. Wesolowski, EPL **95**, 56001 (2011).

[23] H. Kyakuno, K. Matsudaa, H. Yahiro, Y. Inami, T. Fukuoka, Y. Miyata, YanagiK, Y. Maniwa, H. Kataura, T. Saito, M. Yumura and S. Iijima, J. Chem. Phys. **134**, 244501 (2011).

[24] M. Majumber, N. Chopra, R. Andrews and B. J. Hinds, Nature **438**, 44.

[25] A. I. Kolesnikov, J.-M. Zanotti, C. K. Loong, P. Thiyagarajan, A. P. Moravsky, R. O. Loutfy and C. J. Burnham, Phys. Rev. Lett. **93**, 035503 (2004).

[26] E. Bekyarova, Y. Hanzawa, K. Kaneko, J. Silvestre-Albero, A. Sepulveda-Escribano, F. Rodriguez-Reinoso, D. Kasuya, M. Yudasaka and S. Iijima, Chem. Phys. Lett. **366**, 463 (2002).

[27] K. Murata, K. Kaneko, W. A. Steele, F. Kokai, K. Takahashi, D. Kasuya, M. Yudasaka and S. Iijima, Nanoletters **1**, 197 (2001).

[28] J. Wuttke, Physica B **266**, 112 (1999).

[29] J. Wuttke, A. Budwig, M. Drochner, H. Kämmerling, F.-J. Kayser, H. Kleines, L. C. Pardo, M. Prager, V. Ossovyi, D. Richter, G. J. Schneider, H. Schneider and S. Staringer, Rev. Sci. Instr. **83**, 075109 (2012).

[30] J. Wuttke and M. Zamponi, Rev. Sci. Instrum. **84**, 115108 (2013).

[31] J. Wuttke, *SLAW: neutron histogram to scattering law converter,* `http://apps.jcns.fz-juelich.de/slaw`.

[32] J. Wuttke, *Frida: Flexible rapid interactive data analysis*, `http://apps.jcns.fz-juelich.de/frida`.

[33] W. Doster, S. Busch, A. M. Gaspar, M. S. Appavou, J. Wuttke and H. Scheer, Phys. Rev. Lett. **104**, 098101 (2010).

[34] J. Wuttke, Algorithms **5**, 604 (2012).

[35] R. Böhmer, K. L. Ngai, C. A. Angell and D. J. Plazek, J. Chem. Phys. **99**, 4201 (1993).

[36] R. Torre, P. Bartolini and R. Righini, Nature **428**, 296 (2004).

[37] A. Wintner, Duke Math. J. **8**, 678 (1941).

[38] GNU Scientific Library, version GSL-1.16, function `gsl_sf_debye_1`.

[39] The smaller q, the narrower the water spectrum. And incidentally, the smallest four values of q belong to out-of-backscattering detectors with reduced resolution. As a result, the elastic scattering at these q may comprise some water contribution that persists up to the highest measured T and thereby corrupts our fitted $F_{\mathrm{horns}}(q,T)$.

[40] J. Wuttke, I. Chang, O. G. Randl, F. Fujara and W. Petry, Phys. Rev. E **54**, 5364 (1996).

[41] J. C. Phillips, Phys. Rev. E **53**, 1732 (1996).

[42] A. Shekhar, R. K. Kalia, A. Nakano, P. Vashishta, C. K. Alm and A. Malthe-Sørenssen, Appl. Phys. Lett. **105**, 161907 (2014).

[43] W. S. Price, H. Ide and Y. Arata, J. Phys. Chem. A **103**, 448 (1999).

[44] J. Qvist, H. Schober and B. Halle, J. Chem. Phys. **134**, 144508 (2011).

[45] R. Hempelmann, *Quasielastic Neutron Scattering and Solid State Diffusion*, Clarendon Press: Oxford (2000).

[46] E. Rössler, Phys. Rev. Lett. **65**, 1595 (1990).

[47] J. Swenson, Phys. Rev. Lett. **97**, 189801 (2006).

[48] S. Khodadadi, S. Pawlus, J. H. Roh, V. García Sakai, E. Mamontov and A. P. Sokolov, J. Chem. Phys. **128**, 195106 (2008).

[49] A. Faraone, L. Liu, C.-Y. Mou, C.-W. Yen and S.-H. Chen, J. Chem. Phys. **121**, 10843 (2004).

[50] H. Tanaka, J. Chem. Phys. **105**, 5099 (1996).

[51] L. Xu, P. Kumar, S. V. Buldyrev, S.-H. Chen, P. H. Poole, F. Sciortino and H. E. Stanley, Proc. Natl. Acad. Sci. USA **102**, 16558 (2005).

[52] P. H. Poole, F. Sciortino, U. Essmann and H. E. Stanley, Nature **360**, 324 (1992).

[53] S. Cerveny, J. Colmenero and A. Alegría, Phys. Rev. Lett. **97**, 189802 (2006).

[54] S. A. Lusceac, M. R. Vogel and C. R. Herbers, Biochim. Biophys. Acta **1804**, 41 (2010).

[55] S. Capaccioli and K. L. Ngai, J. Chem. Phys. **135**, 104504 (2011).

[56] J. Swenson, H. Jansson and R. Bergman, Phys. Rev. Lett. **96**, 247802 (2006).

[57] J. Swenson, H. Jansson, J. Hedström and R. Bergman, J. Phys. Condens. Matter **19**, 205109 (2007).

[58] C. L. Kane, E. J. Mele, R. S. Lee, J. E. Fischer, P. Petit, H. Dai, A. Thess, R. E. Smalley, A. R. M. Verschueren, S. J. Tans and C. Deker, Europhys. Lett. **41**, 683 (1998).

[59] P. Flubacher, A. J. Leadbetter and J. A. Morrison, J. Chem. Phys. **33**, 1751 (1960).